Gamma-ray Signatures for Identifying Plutonium Content Changes in Molten Salt Reactors

Branko Kovacevic[1], Andre Vidal Soares[1], William Walters[1], Azaree Lintereur[1], Benjamin Betzler[2], Louise G. Evans[2], Michael P. Dion[2], Amanda Johnsen[1]

[1]Ken and Mary Alice Lindquist Department of Nuclear Engineering, Penn State University, University Park, PA

[2]Oak Ridge National Laboratory, Oak Ridge, Tennessee, United States

ABSTRACT

Liquid-fueled Molten Salt Reactors (MSRs) are a popular reactor concept for many reasons, but one of the outstanding challenges is nuclear material accounting for nuclear safeguards. Online processing of the nuclear fuel-moderator mixture introduces pathways for potential nuclear material diversion and the liquid, semi-homogenous nature of the molten salt fuel precludes any ability to count discrete items or fuel elements, such as rods or assemblies. Thus, safeguarding of MSRs will require the development of MSR-specific nuclear material diversion detection strategies. To address the need for reliable identification of diversion signatures and associated quantitative measurement methods, we have developed a model of the Molten Salt Demonstration Reactor (MSDR) modified to use low-enriched uranium (LEU) fuel to investigate the effect of changes in Pu content. For neutronics and burnup modeling, we used the Monte Carlo code Serpent, which has recently added the capability to model continuous feed and removal of nuclides, as is required for the analysis of most MSR designs. For this work, the model was used to simulate the effects of various Pu concentrations in the salt and their effect on isotopic inventories. As a preliminary examination of possible diversion signatures, GADRAS was used to quantify variations in the observed gamma-ray spectral lines in response to changes in the isotopic inventory. These results have revealed potential isotopes of interest that correlate with changes in Pu content within the fuel, such as ^{91m}Y, ^{91}Sr, ^{92}Sr, ^{106}Tc, and ^{136}Cs. For a test case with a reduction of Pu content by 5.5 %, these fission products differed from the reference case in the range of 0.9 to 2.2%. These nuclides also had gamma ray peaks that were well above the Compton continuum and without significant interference from nearby photopeaks.

INTRODUCTION

Molten Salt Reactors (MSRs) have gained significant global interest in recent years due to their potential improvements over light water reactors in terms of safety margins, fuel utilization, and economics [1].While MSRs are a promising reactor concept, technical challenges exist, including nuclear material accounting for nuclear safeguards. A nuclear material accounting strategy, particularly for MSR concepts that include online processing of the molten salt fuel, will need to be developed. The coupling of the reactor and chemical processing, as well as the continual feed and removal of nuclear material, present unique challenges to material accounting measures such as the high-temperature and high-radiation environment [2]. The liquid, quasi-homogenous nature of some MSR fuels preclude the ability to count the traditional, discrete amounts of used fuel, such as rods or assemblies, that are easily tracked in most current reactor designs [3].

As a result, liquid-fuel MSRs eliminate many traditional nuclear fuel accountancy methods. Further, the use of liquid fuel and the system components supporting operational functions, like an off-gas system, also expand the types of nuclear material signatures and signature detection techniques available for accountancy efforts. The off-gas system may enable the use of online, near real time mass spectrometry techniques [4]; chemically separated fuel streams in some concepts may enable increased use of gamma-ray spectroscopy to monitor certain isotopes [2] because there will be less interference from other gamma-ray emitting nuclides . Further, unlike

for a light water reactor fuel assembly, geometries favorable for detection could be built into the process stream.

In this paper, we present our initial, computational modeling-based evaluations of liquid fuel MSR gamma-ray signature changes caused by Pu diversion. Specifically, we examine how the protracted removal of Pu from the fuel salt will change the fission product inventory and how sensitive gamma ray spectroscopy techniques are to those changes. Reactor depletion modeling was performed using Serpent [6] and the resulting gamma-ray signatures were modeled using GADRAS [7] software. Modeling was performed for both normal reactor operation and different rates of abnormal nuclear material removal representing illicit material diversions. The modeled gamma-ray spectroscopic responses that arise from various material diversion scenarios are compared to the nominal reference scenario. Quantification of spectroscopic differences will enable identification of changes that appear as a result of illicit Pu diversion.

We note that this study focuses on a thermal LEU fuel cycle and the variation of Pu concentrations. Many different fuel cycles have been proposed for MSRs. A thorium fuel cycle or natural U-fed fast reactor cycle may require a different approach than discussed here. Several other researchers also have ongoing efforts on MSR material accounting [8].

REACTOR MODEL

The simulations presented are built on the previous reactor modeling work by this team [9], which was based on the graphite-moderated MSDR[10]. In this work, the model was adjusted to use a lower initial enrichment (2.75 w% U-235) and longer fuel cycle (8 years) to more closely resemble recent proposed fuel cycles (e.g., [11]). The reactor model was constructed using the Monte Carlo Code Serpent [6]. The simplified reactor schematic showing the reactor and material flows can be seen in Figure 1.

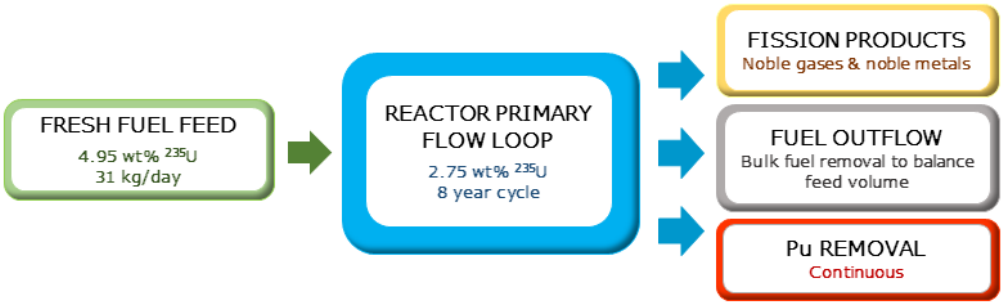

Figure 1: Schematic of the MSR Serpent model constructed for this work including material flows.

The modeled reactor is fueled with LiF-UF_4 (72.5 – 27.5 mol%) and simulated for an 8-year fuel cycle at a power of 750 MWt and achieves a burnup of 11.9 MWd/kg of total initial U mass. Fission product gases, which are generally insoluble in the salt are removed on a 42 minute cycle based on previous studies [12]; the gases removed in this stream are: He, N, O, Ar, Kr and Xe. A set of noble metals also face solubility issues in the salt and have a tendency to plate out at various reactor locations. The noble metals removed in the reactor simulation are Se, Nb, Mo, Tc, Ru, Rh, Pd, Ag, Sb and Te, at a rate equivalent to a 42 minute cycle [12]. Protracted diversion scenarios of Pu were simulated using different rates which were chosen such that 0, 1, and 10 significant quantities (SQs, i.e., 0, 8, and 80 kg of Pu, respectively) were removed by the end of the 8-year cycle.

PREDICTED EFFECTS OF PLUTONIUM REMOVAL

The U-fed reactor design will inevitably have a rising number of Pu fissions throughout its lifetime due to the buildup of ^{239}Pu from neutron capture by ^{238}U. These Pu fissions will affect the fission

product inventories within the fuel salt over time because thermal fission products of ^{235}U and ^{239}Pu differ significantly, as shown in Figure 2.

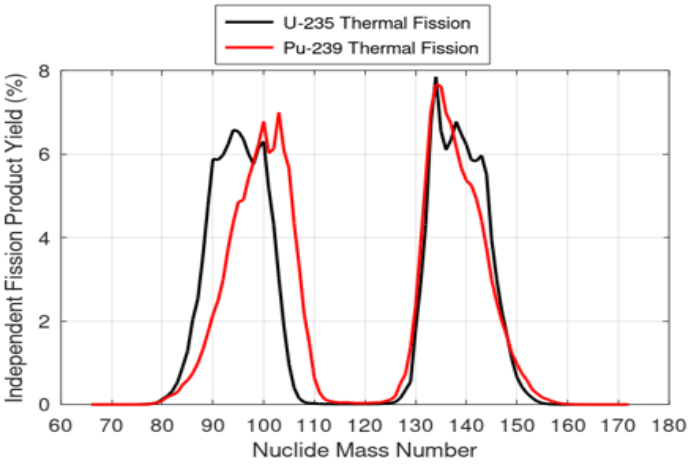

Figure 2: Independent thermal fission yields of ^{235}U and ^{239}Pu [https://www-nds.iaea.org/exfor/endf.htm]

It is clear from Figure 2 that fissions from ^{235}U will favor the production of isotopes with mass numbers between 85 and 95 and between 140 to 145, while those with mass numbers between 103 to 112 and 135 to 138 are favored in ^{239}Pu fissions. Therefore, illicit removal of Pu from the reactor should shift the production of these isotopes away from their ratios attained through normal reactor operation and will have the greatest effect in the mass ranges described above. Since we are modeling continual removal of Pu, the changes in atom density of these fission product isotopes should accumulate up to the end of the reactor lifetime.

The fission product concentration differences driven by their yields, allow the prediction of associated gamma-ray emission lines that could be indicators of Pu removal. Promising candidate isotopes would require a large difference between the U and Pu fission product yields, a large gamma-ray intensity, and preferably a high gamma-ray energy, to reduce interference from the collective Compton plateau from other gamma-ray emissions. We used these characteristics to define the metric, *M*, shown below.

$$M = \frac{(\gamma_U - \gamma_{Pu})^2}{(\gamma_U + \gamma_{Pu})^{\frac{3}{2}}} \left(\frac{E_\gamma}{E_0}\right) I_\gamma$$

Here, γ_U and γ_{Pu} are the cumulative fission yield of the given nuclide from ^{235}U and ^{239}Pu thermal fission, respectively, E_γ is the energy of a gamma-ray of the given nuclide, E_0 is a constant (1 keV used here), and I_γ is the number of gamma-rays emitted at the given energy per nuclide decay (i.e., the photon emission intensity). Note that the cumulative, not independent, fission yields are used to account for decay into the daughter products.

Table 1 shows all the gamma-ray emitting fission products with a metric score greater than 10 which was chosen to provide a preliminary list of candidate isotopes. The emission lines from these isotopes are expected to produce the greatest gamma-ray peak area differences in simulated GADRAS spectra created from Serpent results. Note that the metric does not account for the presence of other strong gamma-ray emitters that could overpower the signatures in Table 1 because of spectrum crowding, but it provides a preliminary picture of expected signature results PyNE[13] was used to process gamma-ray data with fission yield data from ENDF/B-VIII.0 [14].

Table 1: Fission products with gamma-ray emission lines having metric score greater than 10.

Nuclide	γ_{Pu}, %	γ_U, %	γ_U/γ_{Pu}	**Half-Life**	E_γ, keV	I_γ, %	M
^{88}Kr	1.27	3.55	2.79	2.8 hr	2195.8 2392.1	13.18 34.60	14.2 40.6
^{88}Rb	1.33	3.57	2.69	17.8 min	1836.0	22.81	19.4
^{89}Rb	1.71	4.72	2.76	15.3 min	1031.9 1248.1 2195.9 2570.2	62.90 45.92 14.47 10.69	36.1 31.8 17.7 15.3
^{91}Sr	2.48	5.83	2.35	9.6 hr	1024.3	33.50	16.0
^{92}Sr	2.96	5.94	2.00	2.6 hr	1383.9	90.00	41.5
^{91m}Y	1.44	3.38	2.34	49.7 min	555.6	95.00	18.7
^{104}Tc	6.07	1.88	0.31	18.3 min	358.0 1676.8	89.00 7.83	25.0 10.3
^{103}Ru	6.99	3.03	0.43	39.2 days	497.1	91.00	22.4
^{105}Ru	5.64	0.96	0.17	4.4 hr	469.4 676.4 724.3	17.55 15.66 47.30	10.6 13.7 44.2
^{107}Rh	3.33	0.15	0.04	21.7 min	302.8	66.00	31.3
^{129}Sb	1.37	0.54	0.40	4.4 hr	813	48.20	10.1
^{136}Cs	0.097	0.006	0.06	13 days	818.5 1048.1	99.70 79.76	20.9 21.4

ISOTOPIC CHANGES

Before modeling potential gamma-ray signatures in GADRAS, we confirmed that the Serpent model results demonstrated the expected trends in atom density changes. Figure 3a shows changes in Pu and ^{235}U content caused by 10 SQ of Pu removal and Figure 3b demonstrates how the fraction of fissions coming from Pu and U differ throughout the reactor operating cycle as well as the effects caused by Pu removal.

Figure 3c results correspond to the predictions made from Figure 2, as U-favored fission products ^{89}Rb and ^{88}Kr see their atom densities rise with 10 SQ removal of Pu. Favored in Pu fissions, such as ^{104}Tc and ^{106}Ru, see their concentrations decrease with the removal of Pu. It is also apparent that the greatest difference in Pu content is at the end of reactor cycle. Therefore, the gamma-ray signatures that follow were examined at the end of the fuel cycle, even though this method can be used when a smaller amount of Pu diversion has occurred.

Figure 3d shows the k-eff changes in the system over the cycle. Note that the removal of Pu actually results in an increase in k-eff due to the high thermal utilization in the system and the relatively lower thermal reproduction factor in Pu compared to U.

Reactor simulations in Serpent used 150,000 particles and 200 cycles for each scenario, which proved sufficient to achieve consistent model output behavior. All simulations were repeated 12 times independently in order to calculate the stochastic uncertainty in the resulting compositions. The case with no Pu removal was used as the reference, while the 1 SQ and 10 SQ Pu removal cases were used to determine the deviations from the no removal (reference) scenario. Note that since the fission product isotopic changes from 1 SQ Pu removal over 8 years were small, for illustrative purposes all results shown here concern the removal of 10 SQ of Pu over the 8-year reactor operation. Table 2 shows the resulting changes in concentrations and 1-sigma uncertainties of emitters shown in Table 1 caused by different Pu removal rates.

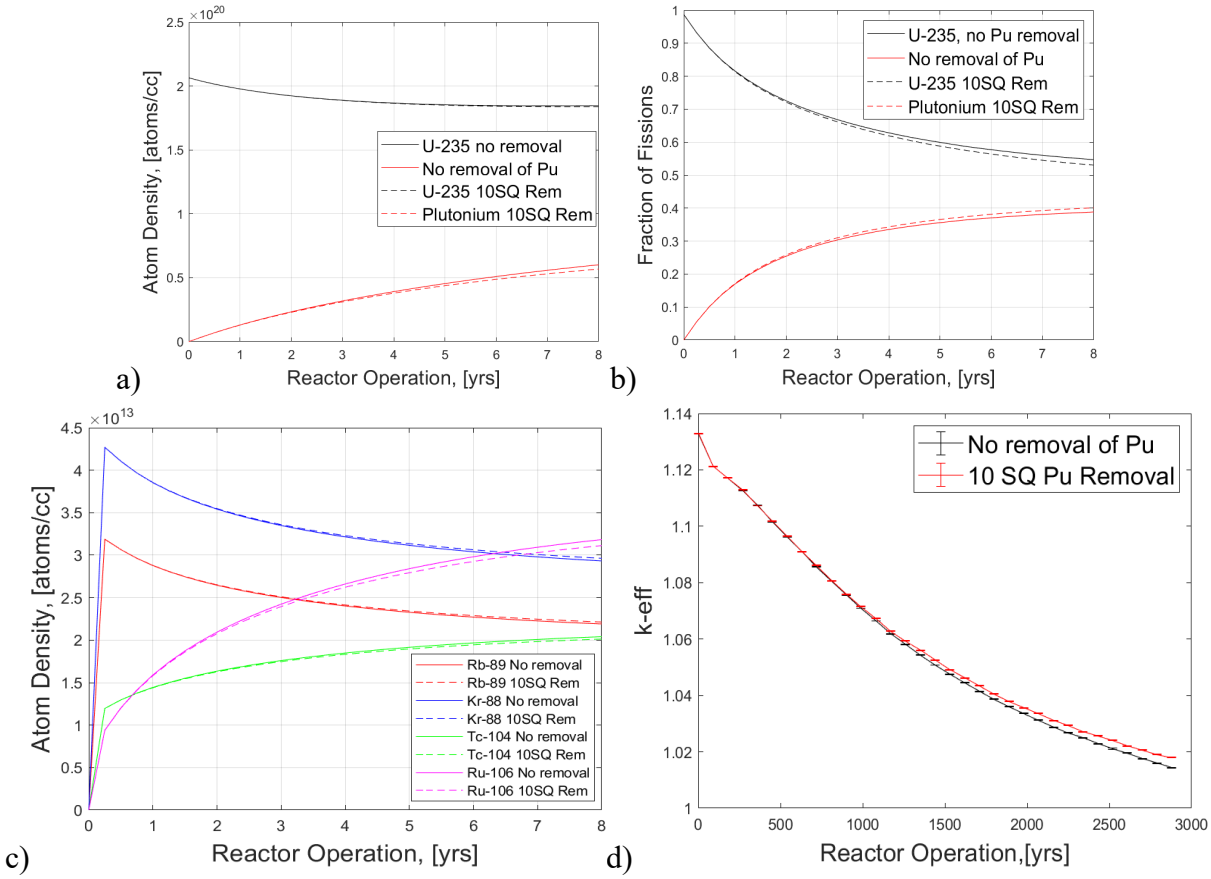

Figure 3. Changes over the reactor lifetime between no Pu removal and 10 SQ Pu removal scenarios: (a) ^{235}U and ^{239}Pu atom density; (b) number of fissions originating from ^{235}U and ^{239}Pu; and (c) fission product atom density, d) k-eff. Isotopes reach equilibria within the first time step

Table 2: Changes in concentration of select gamma emitters as modeled through muliple Serpent runs at the end of the cycle with 10 SQ and 1 SQ Pu removal.

Isotope	Atom density change, %	
	10 SQ Pu removal	1 SQ Pu removal
^{TOTAL}Pu	-5.54 +/-0.003	-0.55 +/- 0.005
^{88}Kr	1.05 +/-0.005	0.10 +/- 0.004
^{88}Rb	0.87 +/-0.004	0.08 +/- 0.004
^{89}Rb	1.05 +/-0.005	0.10 +/- 0.004
^{91}Sr	0.91 +/-0.004	0.08 +/- 0.004
^{92}Sr	0.76 +/-0.004	0.07 +/- 0.004
^{91m}Y	0.91 +/-0.004	0.08 +/- 0.004
^{104}Tc	-1.37 +/-0.003	-0.13 +/- 0.005
^{103}Ru	-0.98 +/-0.002	-0.09 +/- 0.004
^{105}Ru	-1.80 +/-0.004	-0.17 +/- 0.007
^{107}Rh	-2.46 +/-0.003	-0.24 +/- 0.010
^{129}Sb	-0.95 +/-0.002	-0.09 +/- 0.004
^{136}Cs	-1.65 +/-0.017	-0.17 +/- 0.019

The changes in atom density of these isotopes are in agreement with the qualitative predictions made previously based on the fission yields shown in Figure 2. These changes in atom density may drive the subsequent differences in gamma-ray signatures, as emission lines for these isotopes

will show the same relative differences in intensity thus creating deviations in the gamma spectra as Pu is being removed from the reactor. Some additional emitters might appear in the signatures because of the conditions used for the predictive metric.

It should be noted that there are also large differences in the concentration of most actinides such as Pu, Np, Am, and Cm, but their gamma-ray signatures are generally lower in intensity and energy than those of the fission products.

GADRAS METHODOLOGY

After the 8 year reactor simulation time, a series of decay steps were also simulated with the sample. Decay times of 0, 1.2 hrs, 2.4 hrs, 12 hrs, 1.5 days and 5 days were used to examine the changes in gamma-ray signatures after removal from the reactor, as might be expected if a small sample of fuel salt was removed for inspection. The results from these decay steps were used as source inputs in GADRAS to simulate a high purity germanium (HPGe) detector response. A full spectrum up to 3000 keV is shown in Figure 4 for the baseline case and with 10 SQ removal with no decay time.

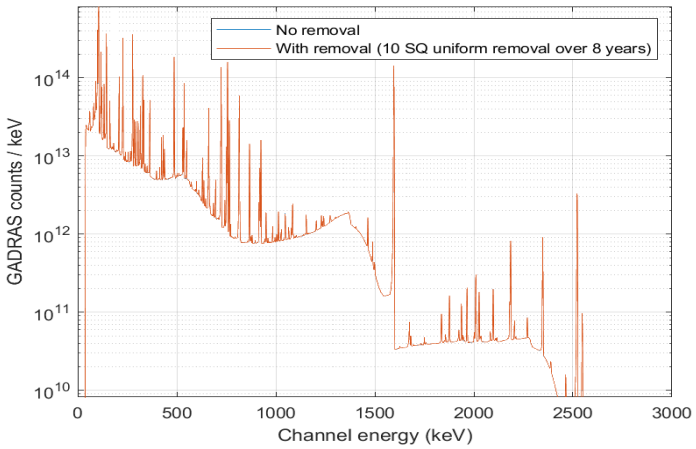

Figure 4: HPGe detector GADRAS response Spectra. No Pu removal (reference) case in red and 10 SQ Pu removal in green at the end of the 8-year cycle. The differences are very subtle when looking at the entire spectra.

The modeled GADRAS detector was a 95% relative efficiency HPGe detector with no deadtime. For detector response uncertainty analysis, the source was scaled to 1 Ci to represent a reasonable measurement activity.

The sources with no Pu removal were plotted against the sources produced from various Pu removal rates; all comparisons were made at identical time steps. An algorithm was written in Matlab to identify gamma-ray peaks within the modeled GADRAS spectra corresponding to specific fission products. The algorithm detects local maxima above a threshold to determine the existence and location of peaks. Once all peaks matching the algorithm criteria are identified, two metrics are used to evaluate those peaks for use as possible signatures. First, a Peak-to-Baseline ratio is calculated, where the peak value is the maximum height, while the baseline is the average number of counts per channel that make up the Compton continuum underneath the peak, as shown in Figure 5. The second metric is the Compton subtracted peak area, which is defined as the sum of the counts in all peak channels minus the sum of the counts below the Compton continuum.

GADRAS RESULTS AND DISCUSSION

The gamma-ray modeling results and the spectral differences between material removal scenarios will depend on an individual process stream and on the time step used in the analysis. This initial

analysis examines only the responses from the reactor primary fuel loop (Figure 1), not the separation streams.

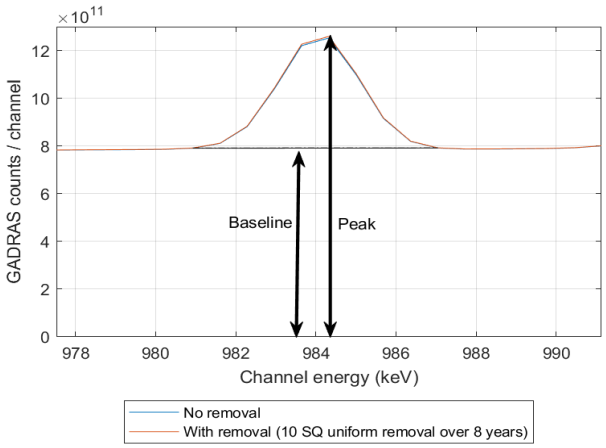

Figure 5: Illustration of the Compton subtraction and Peak-to-Baseline metric for a sample gamma-ray peak from GADRAS

Figure 6 and Figure 7 summarize the gamma-ray peak analyses conducted on modeled GADRAS spectra for the 'no Pu removal' and the 10 SQ removal scenarios for the reactor primary fuel loop. Each of these figures shows gamma-ray energies versus the relative count difference at those energies between the baseline and 10 SQ Pu removal scenarios. Each figure represents a unique time step after a 'sample' of the fuel salt has been removed from the reactor. The values noted in the gray boxes correspond to the identity of the nuclide of interest, the peak area difference (metric 2), and the Peak-to-Baseline ratio (metric 1).

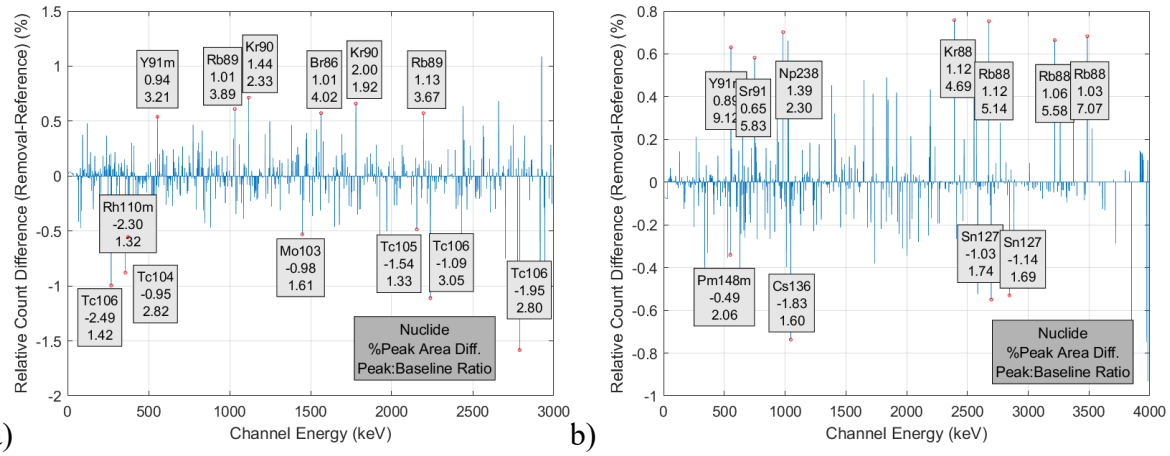

a) b)

Figure 6: Notable peak area differences between the baseline case and signatures created by linear removal of 10 SQ of Pu over the period of 8 years. Y-axis shows differences in the number of counts per channel. (a) Source without decay. Cut-offs used: >0.85% difference and >1.3 PBR; (b) Source decayed 12 hours. Cut-offs used: >0.65% difference and >1.3 PBR

Figure 6 and examination of results from other time steps show that the peaks are created by several isotopes that are capable of dominating the spectrum in a certain time step, so isotopes with half-lives on the order of seconds and minutes dominate the spectra produced with an undecayed source, while the spectra of the 12-hour decayed source are dominated by isotopes with half-lives in the range of hours. There are also several instances of high differences in the number of counts per channel (y-axis), but these were not selected because the peaks' Peak-to-Baseline Ratio was very small which implies they are hardly visible and their area uncertainty is also very high.

Table 3 summarizes the best peaks that appear in the decay steps we examined based on the following criteria: high peak area difference caused by Pu removal, relatively high Peak-to-Baseline Ratio (this lowers the peak area uncertainty as well) and matching of the calculated peak area difference and difference in the activity of the emitting isotope that dominates the peak. Generally, peaks with a higher Peak-to-Baseline values tended to have better agreement between the atom density differences and peak area differences.

Table 3: Summary of select gamma-ray peaks that satisfied peak identification conditions and had a significant peak area percent difference between the baseline and 10 SQ Pu removal.

GADRAS Peak Energy channel, keV	Dominant Isotope	Time range when peak is identifiable, days	Highest Peak-to-Baseline Ratio	Peak Area, % Difference	Dominant Isotope Atom Density, % Difference
269.5	^{106}Tc	0	1.44	-2.73	-2.21
555.2	^{91m}Y	0 to 0.5	10.23	0.89	0.91
629.7	^{148m}Pm	5	3.82	-0.86	-0.73
749.7	^{91}Sr	0.05 to 0.5	5.39	0.89	0.91
1023.8	^{91}Sr	0.05 to 0.5	12.96	0.78	0.91
1031.2	^{89}Rb	0	3.85	1.01	1.05
1047.9	^{136}Cs	5	2.09	-1.59	-1.64
1383.6	^{92}Sr	0.05 to 0.1	32.07	0.76	0.76
1564.6	^{86}Br	0	3.99	0.97	1.03
2570.2	^{89}Rb	0.05	4.06	1.08	1.05

Early gamma-ray signatures are dominated by isotopes with a short half-life such as ^{86}Br and ^{106}Tc, which decay away very quickly. At longer decay steps all of the peaks are formed by isotopes such as ^{148m}Pm and ^{136}Cs which have half-lives of at least two days. There is also a group of isotopes with high U-favored cumulative fission yields, favorable gamma-ray energies, and high gamma-ray intensities with half-lives from an hour to several hours that are present in signatures across the intermediate decay steps. Isotopes that are particularly responsible for visible peaks are ^{91m}Y, which has a 555 keV photon emission that stays relevant over a wide range of decay steps, and ^{91}Sr and ^{89}Rb, which have a very large number of peaks identified in this analysis.

Some of the isotopes and gamma-ray emission lines visible in Figure 6 were not identified by the metric shown in Table 1 because they had low cumulative fission yields like ^{148m}Pm, or because they had short half-lives like ^{106}Tc. Future work will refine the metric to account for other influencing characteristics and increase its reliability in predicting key fission product signatures.

DETECTABILITY OF GAMMA-RAY SIGNATURES

It is important to estimate whether the differences we found could be detected so we examined the relationship between the differences and their associated uncertainty. Although there are many factors that contribute to the uncertainty of peak areas, the focus here will be on the uncertainty caused by Poisson statistics. This uncertainty was estimated by choosing a sample of provisional size and activity and a feasible count time to estimate the number of counts that would be detected in each peak of interest. We chose to use a fuel salt sample with 1 Ci of activity as a benchmark while noting that this activity might be too high for some measurement scenarios. The counting time was set to 1 hour because most emitters found in the signatures have half-lives on the order of several hours.

Table 4: Uncertainty analysis of Compton-subtracted peak areas for the case of 10 SQ Pu removal sample of 1 Curie of activity, decayed 1.2 hours. Count time is 3600 seconds.

Peak channel energy, keV	Dominant Isotope	Total number of Counts in Peak	Number of Compton Subtracted Counts	Peak Area Uncertainty, %	Peak Area Difference, %
555.2	^{91m}Y	2,778,541	438,856	0.08	0.89
749.7	^{91}Sr	1,098,268	366,374	0.18	1.05
1023.8	^{91}Sr	1,053,473	132,823	0.13	0.83
1383.6	^{92}Sr	1,855,367	81,165	0.08	0.76
1835.9	^{88}Rb	45,349	16,287	1.06	1.15
2195.7	^{88}Kr	31,902	11,156	1.12	1.07
2483.4	^{84}Br	6,738	3,255	3.45	0.91
2569.8	^{89}Rb	7,382	2,152	2.10	1.08
2695.7	^{127}Sn	2,729	1,889	7.96	-0.62

Table 4 illustrates that detector uncertainty can be within the limits of peak area differences between the baseline and 10 SQ removal cases for some of the lower energy peaks with a higher Peak-to-Baseline Ratio for the given conditions. Such peaks will have a much greater chance of being useful signatures for detecting Pu diversion. These statistics will certainly be different based on the sample activity and count time chosen and those can be variable depending on the decay step.

The detector Poisson uncertainty calculated here was shown for a 10 SQ diversion case. Looking at any one of these signatures, the removal of 1 SQ would be challenging to detect from solely a Poisson-statistics point of view, let alone from other sources of uncertainty in the detector, modeling assumptions, or nuclear data. However, the synthesis of signatures from many peaks and/or isotopes should greatly improve the detectability and will be an important area of future research.

CONCLUSION

This paper examined the gamma-ray signatures that correlate with removal of Pu from an LEU-fueled thermal spectrum MSR. Reactor simulations performed using Serpent verified that removing Pu from the system results in an increase in U-favored fission products and a decrease in Pu-favored fission products linearly with the amount of Pu removed. Idealized HPGe gamma-ray detector simulations using GADRAS showed that small differences may be noticeable in many gamma-ray peaks visible at different decay times of a sample. Many peaks are well-isolated from interference from other peaks and showed differences in calculated peak area very close to the predicted isotopic differences. The most promising gamma-ray emitting nuclides noted here included ^{91m}Y, ^{91}Sr, ^{92}Sr, ^{106}Tc, and ^{136}Cs. Changes due to gamma-rays from higher actinides were not visible except for ^{238}Np for some decay times. Future studies will include looking at the various other material streams (e.g., the noble metal and off-gas), different Pu removal strategies (e.g., abrupt vs protracted), earlier detection of Pu removal, other signatures (e.g., neutron multiplicity), the synthesis of various signatures (e.g., various gamma-ray lines) to improve detectability, and an assessment of nuclear data uncertainty.

ACKNOWLEDGMENTS

This material is based upon work supported by a Department of Energy Nuclear Energy University Program under award CFA-19-17395. We would also like to thank Nathan Shoman for his valuable feedback on this project.

REFERENCES

[1] D. Petti *et al.*, "A Summary of the Department of Energy's Advanced Demonstration and Test Reactor Options Study," *Nucl. Technol.*, vol. 199, no. 2, pp. 111–128, Aug. 2017, doi: 10.1080/00295450.2017.1336029.

[2] A. Worrall *et al.*, "Molten Salt Reactors and Associated Safeguards Challenges and Opportunities," Art. no. IAEA-CN--267, 2018, Accessed: Jul. 01, 2021. [Online]. Available: http://inis.iaea.org/Search/search.aspx?orig_q=RN:51003743

[3] D. N. Kovacic *et al.*, "Safeguards Challenges for Molten Salt Reactors," Oak Ridge National Lab. (ORNL), Oak Ridge, TN (United States), Aug. 2018. Accessed: Jul. 01, 2021. [Online]. Available: https://www.osti.gov/biblio/1474868-safeguards-challenges-molten-salt-reactors

[4] N. Shoman and B. B. Cipiti, "MSR Safeguards Modeling Efforts.," Sandia National Lab. (SNL-NM), Albuquerque, NM (United States), SAND2019-4350PE, Apr. 2019. Accessed: Jul. 01, 2021. [Online]. Available: https://www.osti.gov/biblio/1644918-msr-safeguards-modeling-efforts

[5] S. Garti *et al.*, "Characterizing low-activity waste containers: A case study for Compton Suppression Systems under challenging signal-to-noise ratio," *Nucl. Instrum. Methods Phys. Res. Sect. Accel. Spectrometers Detect. Assoc. Equip.*, vol. 949, p. 162806, Jan. 2020, doi: 10.1016/j.nima.2019.162806.

[6] J. Leppänen, M. Pusa, T. Viitanen, V. Valtavirta, and T. Kaltiaisenaho, "The Serpent Monte Carlo code: Status, development and applications in 2013," *Ann. Nucl. Energy*, vol. 82, pp. 142–150, Aug. 2015, doi: 10.1016/j.anucene.2014.08.024.

[7] Steven M. Horne, Gregory G. Thoreson, Lisa A. Theisen, Dean J. Mitchell, Lee T. Harding, and Sean E. O'Brien, *GADRAS Version 18 User's Manual*.

[8] K. Hogue, P. Gibbs, M. Dion, and W. Poore III, "Domestic Safeguards Material Control and Accountancy Considerations for Molten Salt Reactors," ORNL/SPR-2020/1881, 1797666, 150504, Feb. 2021. doi: 10.2172/1797666.

[9] A. Vidal Soares *et al.*, "Nuclear data uncertainty challenges in Molten Salt Reactor safeguards," Oak Ridge National Lab. (ORNL), Oak Ridge, TN (United States), Nov. 2020. Accessed: Jul. 08, 2021. [Online]. Available: https://www.osti.gov/biblio/1763462

[10] M. S. Greenwood, B. R. Betzler, and A. L. Qualls, "Dynamic System Models for Informing Licensing and Safeguards Investigations of Molten Salt Reactors," Oak Ridge National Lab. (ORNL), Oak Ridge, TN (United States), ORNL/TM-2018/876, Jun. 2018. doi: 10.2172/1456790.

[11] J. Choe, M. Ivanova, D. LeBlanc, S. Mohaptra, and R. Robinson, "FUEL CYCLE FLEXIBILITY OF TERRESTRIAL ENERGY'S INTEGRAL MOLTEN SALT REACTOR (IMSR®)," p. 13, 2018.

[12] P. Jr Vicente Valdez, B. R. Betzler, W. Wieselquist, and M. Fratoni, "Modeling Molten Salt Reactor Fission Product Removal with SCALE," ORNL/TM-2019/1418, 1608211, Mar. 2020. doi: 10.2172/1608211.

[13] C. R. Bates *et al.*, "PyNE progress report," in *Transactions of the American Nuclear Society*, Jan. 2014, vol. 111, pp. 1165–1168. Accessed: Jul. 19, 2021. [Online]. Available: https://experts.illinois.edu/en/publications/pyne-progress-report

[14] D. A. Brown *et al.*, "ENDF/B-VIII.0: The 8th Major Release of the Nuclear Reaction Data Library with CIELO-project Cross Sections, New Standards and Thermal Scattering Data," *Nucl. Data Sheets*, vol. 148, pp. 1–142, Feb. 2018, doi: 10.1016/j.nds.2018.02.001.